Tendon-Driven Robotic Arm Control Method Based on Radial Basis Function Adaptive Tracking Algorithm

Xiaoke Fang
College of Information Science and Engineering, Northeastern University, Shenyang 110004, China

***Abstract*—With the rapid development of intelligent technology, robotic arms are widely used in different fields. The study combines the tendon drive theory and radial basis function neural network to construct the robotic arm model, and then combines the back-stepping method and non-singular fast terminal sliding mode to improve the controller and system optimization of the tendon drive robotic arm model. Simulation tests on commercial mathematical software platforms yielded that joint 2 achieves stable overlap of position trajectory and velocity trajectory after 0.2s and 0.5s with errors of 1° and 1°/s, respectively. Radial basis function neural network approximation of robotic arm error converged to the true value at 14s. The optimized joint achieved the accuracy of trajectory tracking after 0.2s. Also the control torque of joint 2 changes at 1.5s, 4.5s and 8s and its change is small. The tendon tension curve was smoother and more stable in the range of -0.05N~0.0.5N to show that the robotic arm model has superiority after the optimization of the controller, and the interference observer had accurate estimation of the tracking trajectory of the tendon-driven robotic arm. Therefore, the radial basis function-based adaptive tracking algorithm had higher accuracy for the tendon-driven robotic arm model and provided technical reference for the control system of the intelligent robotic arm.**

Keywords*—Tendon drive; adaptive neural network; dynamic relationship; sliding membrane control; trajectory tracking

I. Introduction

Robot arm (RA) is a device that is programmed to move and manipulate a manipulator to perform a grasp-and-place operation [1]. With the development of computers, RAs are used in engineering fields such as ecosystem monitoring, aerospace and medical engineering [2-4]. RA, as an important component in robotic systems, can perform working robot control such as industrial assembly, safety and explosion prevention, and medical assistance [5]. Robot control lies in motion and dynamics, and RA, as a nonlinear system, is characterized by strong coupling and multivariate variables, and is easily affected by multiple uncertainties. The precise control of its joint angles and trajectory tracking (TT) requires the RA model to address the dynamics modeling errors, uncertain external disturbances, and unknown parameters, and then design controllers to improve the accuracy, stability, and flexibility of RA grasping [6-7]. And for the automation application technology of RA, its movement, grasping, obstacle avoidance and other aspects of the model construction, and according to the industrial needs of different forms of RA or robots for the assembly or intelligent improvement. Among the RA's TT in mechanical structure, controller and other aspects of performance interference, so for the intelligent control method of RA, combined with the human arm structure of the apparatus to design. However, when the environment changes or complex parameters are generated, the motion control parameters of the robotic arm are limited by many factors, which poses significant challenges in automated operations. Control algorithms are currently the technological means for intelligent application of industrial robotic arms, and the feasibility of their motion control performance is ensured through precise parameters of robotic arm dynamics modeling. Systematic research and optimization are carried out in the areas of RA adaptive control and sliding mode control to solve the application problems of RA movement, control and grasping. To accurately establish the dynamic parameters of the robotic arm, the study utilizes tendon drive theory to explain the kinematic relationship between joints and displacement, in order to enhance the design and use of the controller. Based on this, the study combines radial basis function (RBF) neural network and controller design to provide an optimization approach for Tendon-driven robotic arm (TDRA) trajectory control method, which in turn improves the accuracy of TT control.

The research is carried out in six sections, Section I is an expository description of the current research results. Related works is given in Section II. Section III is to optimize the control performance of RA using back-stepping and Non-singular Fast Terminal Sliding Mode (NFTSM). Section IV gives detail about the TDRA control combining RBF and controller. Discussion is given in Section V. Finally, Section VI concluded the paper.

II. Related Works

The manufacturing of industrial automation has made extensive use of RA technology. In the realm of intelligent control, TT control of RA systems with uncertainty is a hotspot for research since many applications need RA to follow trajectory motion accurately. Over the last years, scholars at home and abroad have explored the application and improvement of RA. Zhao proposed a robotic arm control system based on multi feature videos regarding the issue of robotic arm grasping, and combined it with a laser rangefinder to verify the success rate of robotic arm grasping. Finally, the accuracy and feasibility of its robotic arm motion control were determined [8]. Yang et al. proposed a method for improving the effectiveness of robot automatic search tasks based on

airborne sensors and wearable embedded systems, combined with localization algorithms and motion control algorithms, regarding the localization and motion control issues of biological robots [9]. For the robot temperature sensing problem, He et al. proposed to implant the temperature sensor into the robot simulation finger using fiber grating, and measured the temperature with the goal to prove the feasibility and effectiveness of their approach [10]. For the tendon-driven manipulator TT problem, Peng et al. suggested to use a fuzzy logic control method and simulation testing of the linearized system, which in turn improves the performance of TT control [11]. Regarding the control system problem of the target grasping robot, Matsuda et al. proposed to use an image processing method and autonomous control of a mobile robot with a distance sensor and an object grasping arm, which in turn improves the accuracy of the robot's object grasping system [12]. Regarding the development of the robot's ability to move trajectory, motion tracking, and object grasping, a number of industrial-type robots have been put into application and effective results have been achieved.

In addition, robots and RA have a wide range of applications in medicine and industry, etc. In terms of robot motion models and TT, many research scholars have used many intelligent means and automation techniques to optimize and improve the model construction. Regarding the application of three-degree-of-freedom robots in medicine, Jiang et al. analyzed surgical robots and proposed using fiber optic sensors to optimize their ability to resist electromagnetic interference in surgical procedures, thereby demonstrating the superiority of surgical robots based on fiber optic and sensing technology [13]. For the application development problem of rehabilitation robots, Liu Y et al. proposed to use a control method based on surface EMG signals and combined with principal component analysis to improve the recognition accuracy, which in turn improves the effect of skeletal rehabilitation training [14]. Linxi et al. proposed a design feature space based on sparse point clouds to distinguish target characters for the tracking problem of outdoor mobile robots, and combined with motion planning algorithms to verify target detection and tracking performance, thereby increasing the robustness of robots to complex outdoor environments [15]. Naya Varela et al. proposed to combine biological morphological development and controllers for the bipedal robot walking problem, and then use neural evolution algorithms to verify the feasibility and practicality of bipedal robot walking [16]. Regarding the robot motion model construction problem, Fei proposed to use a joint torque estimation method based on dynamic characteristics and a traceless Kalman filter to simulate and test the flexibility model, and then prove the effectiveness and feasibility of his method [17].

In summary, although domestic and foreign researchers and scholars have carried out a number of model construction and technology optimization for the application development of RA. However, there is a lack of in-depth research on the widespread movement trajectory and joint flexibility testing for industrial development of robotic applications. At the same time, and existing research on the kinematic parameters such as joint displacement and torque of robotic arms still lacks specific kinematic relationship derivation for their driving models, which affects the dynamic analysis of robotic arms. Therefore, the study innovatively cites the tendon drive theory and its system to enhance the compactness of the robotic arm joint structure, provide more accurate parameter relationships for dynamic modeling, and reduce the load on the joint drive. Afterwards, an RBF-Adaptive neural network (ANN), controller design, and disturbance observer were used to construct TDRA based on the RBF adaptive tracking algorithm, aiming to improve the accuracy of TT control and provide technical reference for the intelligent development of industrial robots.

III. Construction of Robot ARM Control System based on RBF-NN and Tendon Drive

For the construction of Dynamics modeling (DM) of RA, the study combines the tendon drive theory and RBF-NN to build the ANN tracking control system [18]. And according to the nonlinear system with stronger disturbances and its TT problem, the study utilizes back-stepping and fuzzy control to globally control the modeling information of the TDRA in order to achieve accurate and stable TT. Finally, when the external disturbances and errors are large, the disturbance observer is introduced to the sliding membrane control (SMC), which in turn improves the accuracy of the TT.

A. TDRA's Dynamics Modeling and its Tracking Controller

The dynamics of the TDRA includes the analysis of the action and dynamics of the joint displacements, angles and velocities, while the dynamic structure of the RA is simplified to the base, the rear arm linkage and the forearm linkage. Among the commonly used modeling approaches are Lagrangian and Newtonian Eulerian methods, but the dynamics equations are applied consistently in the same system [19]. The most widely modeled approach is the Euler-Lagrange equation, where the RA is represented as shown in Eq. (1).

$$P(j)a + C(s,j)s + G(j) = \tau \tag{1}$$

In Eq. (1), $P(j) \in R^{n \times n}$ denotes the positive definite inertia matrix and n is the joints of the RA, j, s and a are the joint angular displacements, velocities and accelerations, respectively, and $j, s, a \in R^n$. $C(s,j) \in R^{n \times n}$ is the centripetal and Koch force matrix, and $G(j)$ is the gravity matrix and $G(j) \in R^n$. The input moment of the joints is $\tau \in R^n$ and $\tau = (\tau_1, \tau_2, \tau_3)^T$. The Lagrange kinetic equations are used to derive the DM, which leads to the positive definite inertia matrix as shown in Eq. (2).

$$P(j) = \begin{pmatrix} P_{11} & P_{12} & P_{13} \\ P_{21} & P_{22} & P_{23} \\ P_{31} & P_{32} & P_{33} \end{pmatrix} \tag{2}$$

In Eq. (2), $P(j)$ is the positive definite inertia matrix and $P_{12} = P_{13} = P_{21} = P_{31} = 0$. While the centripetal force and

the Koch matrix are expressed as shown in Eq. (3).

$$C(j,s)=\begin{pmatrix} C_{11} & C_{12} & C_{13} \\ C_{21} & C_{22} & C_{23} \\ C_{31} & C_{32} & C_{33} \end{pmatrix} \tag{3}$$

In Eq. (3), $C(s,j)$ is the centripetal and Koch force matrix and $C_{33}=0$. The main motion of TDRA lies in the relationship between joint angle and tendon displacement, end-effector and joint angle displacement and joint torque and tendon tension. Where the mapping matrix of tendon tension to joint torque is shown in Eq. (4).

$$\tau = Rt \quad R=\begin{pmatrix} r_{11} & r_{12} & r_{13} & r_{14} \\ r_{21} & -r_{22} & r_{23} & -r_{24} \\ 0 & 0 & r_{33} & r_{34} \end{pmatrix} \tag{4}$$

In Eq. (4), τ and t are the joint moments and tendon tensions, respectively, and t denotes the column vector consisting of four tendon tensions. R is the mapping matrix from t to τ, where the element r_{ij} is denoted as the radius of the circular surface surrounded by the j th tendon on the i th joint itself and $i=1\sim 3, j=1\sim 4$. And the model results of the tendon actuator output to a specific joint are shown in Fig. 1.

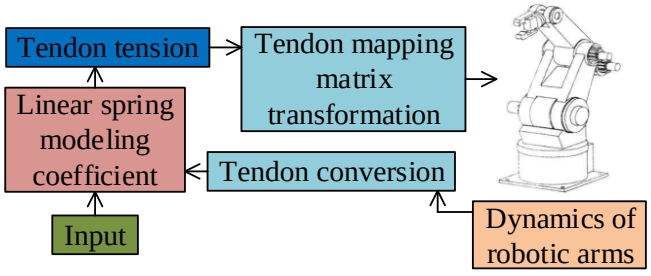

Fig. 1. Schematic diagram of the structure of the tendon actuator output to the joint model.

The input linear spring modeling coefficients can be found in Fig. 1, and the tendon conversion is accomplished in the RA dynamics through the tendon tension and its mapping transformation. The tendon drive combined with RA makes it compact and reduces the load on the joint drive. The tendon drive facilitates controller design by acting as a flexible drive with zero backlash, hence reducing the weight and size of the joint working work. As for the RA tracking control problem under unknown DM, the study combines adaptive control with RBF-NN for modeling and tracking control of TDRA. Among them, RBF-NN has a structure primarily made up of an output layer, a hidden layer, and a hidden input layer. It is a three-layer feed-forward network with a single hidden layer. Among them, the input layer contains a number of signal source nodes, and the nonlinear radial function in the hidden layer, which gradually decreases from the center. RBF is used as the activation function in the hidden layer, which in turn maps the input vector directly to the hidden layer. And the output nodes form the output layer, and then the weight matrix is used to calculate the output value. To solve the constraint problem of RA tendon rope tension, the study uses RBF-NN for the parameters of DM and constructs the tracking control of ANN as demonstrated in Fig. 2.

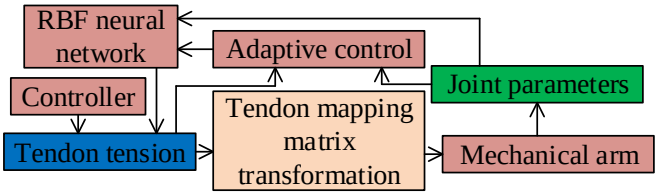

Fig. 2. Adaptive RBF neural network tracking control structure diagram.

From Fig. 2, it is concluded that the DM of TDRA introduces an auxiliary system to solve the tendon tension constraint problem, and the adaptive controller acts on the tendon tension to achieve adaptive control. And through the tendon mapping matrix transformation and RA and its joint parameters, the model information is input to RBF-NN. The RBF-NN controller approaches the unknown dynamic parameters of the RA, which in turn facilitates the optimization of its tracking control performance. According to the RBF-NN's proximity to the unknown dynamical parameters, the DM formulation of its RA, as shown in Eq. (5).

$$\begin{cases} x_1 = j, x_2 = s \\ \dot{x}_1 = x_2 \\ \dot{x}_2 = P^{-1}(x_1)\times\left[\tau - C(x_1,x_2)x_2 - G(x_1)\right] \\ \tau = Rt \end{cases} \tag{5}$$

In Eq. (5), $C(x_1,x_2)$ is the centripetal and Koch force matrix and $G(x_1)$ is the gravity force matrix. And to minimize the effect of tendon rope constraint, the auxiliary system is shown in Eq. (6).

$$A=\begin{cases} -K_\varsigma\varsigma - \dfrac{\left|y_2^T\square f\right| + 0.5\square f^T\square F\times\varsigma}{\|\varsigma\|^2} - \square f & \|\varsigma\|\ge c \\ 0 & \|\varsigma\|\le c \end{cases} \tag{6}$$

In Eq. (6), ς represents the state of the auxiliary system and $\varsigma\in R^{n\times 1}$, and additionally $\begin{cases} K_\varsigma = K_\varsigma^T > 0 \\ \square f = S(f) - f \end{cases}$, the saturation function is modeled as $S(f)=\begin{cases} S_{\max}\,\mathrm{sgn}(x), |f|\ge\tau_0 \\ f, |f|<\tau \end{cases}$, where $S_{\max}$ is the upper saturation limit. The sign function is $\mathrm{sgn}(x)=\begin{cases} 1, x>0 \\ 0, x=0 \\ -1, x<0 \end{cases}$, c is a smaller positive constant. The DM of RBF-NN computes the adaptive law values of the neural network weights, and the model estimates the control law, so improving the robustness

of the error control. Finally, based on the function and the adaptive law value, it is substituted into the auxiliary system, which in turn leads to the DM of the RBF-NN near the TDRA to reduce the error and improve the localization and tracking design of the control system.

B. TDRA Sliding Membrane Control and Trajectory Tracking

It is investigated that the back-stepping approach is utilized for the construction of the adaptive control module to handle the problem of the nonlinear system of RA and TT. This, in turn, solves the problem of uncertain parameters and lack of model information of RA [20]. The back-stepping method is a systematic design method for parameter uncertain systems, which uses a recursive structure to the Lyapunov function of the CLS to obtain the feedback controller. Then combined with the control law of the CLS function derivation, and then make the CLS trajectory and boundedness and convergence to achieve equilibrium. Where Lyapunov function is used in dynamical systems and control systems to analyze the instability and convergence and thus to design their systems efficiently. Thus, Fig. 3 depicts the back-stepping-based TDRA control system construction.

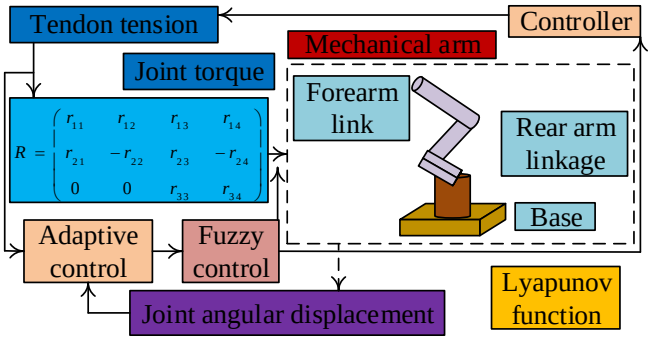

Fig. 3. Structure diagram of control system based on back-stepping method.

The control design of the back-stepping method for TDRA can be seen in Fig. 3. The design effectively approximates the unmodeled information of the RA and solves its parameter uncertainty through the adaptive fuzzy controller and function approximation capability, and then completes the control of the modeled information. Eq. (7) demonstrates the design of the adaptive fuzzy control law.

$$\begin{cases} f = R^{+} \times \left(-\varsigma_2 \varsigma_2 - z_1 - \rho\right) \\ z_1 = y - y_d \end{cases} \tag{7}$$

In Eq. (7), z_1 is the error, y and y_d are the actual and desired angles, respectively, and ρ denotes the fuzzy system design. As for the two subsystems of the controller, its stability analysis is done by using Lyapunov function, as shown in Eq. (8).

$$\begin{cases} L_1 = \dfrac{z_1^T z_1}{2} \\ L_2 = L_1 + \dfrac{z_2^T \times P \times z_2}{2} \end{cases} \tag{8}$$

In Eq. (8), L_1 and L_2 are the function expressions of the two subsystems, z_2 is the error and $z_2 = x_2 - \alpha_1$, α_1 is the estimated value of x_2, and P is the positive definite inertia matrix. The stability analysis of the whole system is derived as shown in Eq. (9).

$$L = L_2 + \frac{\tilde{\beta}^T \tilde{\beta}}{2\lambda} = \frac{z_1^T z_1}{2} + \frac{z_2^T \times P \times z_2}{2} + \frac{\tilde{\beta}^T \tilde{\beta}}{2\lambda} \tag{9}$$

In Eq. (9), β^* of $\tilde{\beta} = \beta^* - \beta$ is the optimal approximation constant, β and λ are constants, and $\lambda > 0$. This is then subjected to derivation and adaptive law substitution into the inequality, as well as boundedness considerations of the disturbances, which ultimately leads to the bounded inequality for the CLS, as shown in Eq. (10).

$$L(t) \le L(0)\exp\left(-C_0 t\right) + \frac{C_{L\max}}{C_0}\left[1 - \exp\left(-C_0 t\right)\right] \le L(0) + \frac{C_{L\max}}{C_0} \tag{10}$$

In Eq. (10), $L(0)$ is the initial value while defining the tight set as $\Omega_0 = \left\{ X \middle| L(X) \le L(0) + \dfrac{C_{L\max}}{C_0} \right\}$ and $\left\{ z_1, z_2, \tilde{\beta} \right\} \in \Omega_0$. Thus it is shown that the system introduced into the controller and its CLS signals are bounded. When uncontrollable external disturbances and large modeling errors occur, it is investigated to design the disturbance observer and place it in the SMC of the RA. The specific structure is shown in Fig. 4.

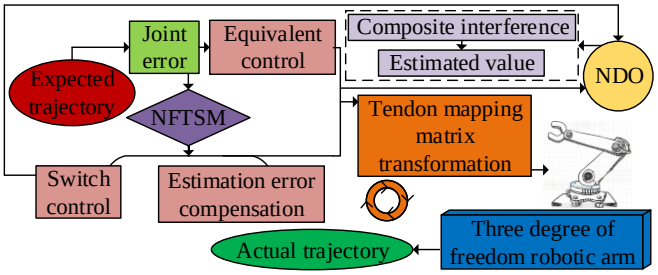

Fig. 4. Design of terminal sliding mode control with anti-interference capability.

In Fig. 4, the errors in inter-joint displacements, velocities and accelerations are used in the equation calculations of the Nonlinear Disturbance Observer (NDO) to determine the errors in the modeled information. To determine the convergence of the errors, the NDO is then constructed along with the auxiliary parameter variables and then merged with the function derivation. Furthermore, the NFTSM provides improved control over the RA motion by compensating for errors, controlling them, and utilizing the saturation function and double power convergence rule. By deliberately altering the switching function, NFTSM, a revolutionary sliding mode control technique, resolves the singularity issue with the current terminal sliding mode control directly from the perspective of sliding mode design and achieves global non-singular control of the system. In the meanwhile, it takes

on the terminal sliding mode's finite-time convergence attribute. When compared to the conventional linear sliding mode control, it can achieve high steady-state accuracy and a finite time convergence to the intended trajectory, making it appropriate for high-speed and high-precision control. Where the TDRA power model considering external disturbances and uncertain parameters, its equation e is shown in Eq. (11).

$$P_0(j)a + C_0(j,s)s + G_0(j) = \tau + \tau_e + \kappa \tag{11}$$

In Eq. (11), κ represents the model uncertainty information and $\kappa = -\Delta P(j)a - \Delta C(j,s)s - \Delta G(j) - F(s)$, $F(s)$ are the system friction forces. τ and τ_e are joint moment vectors and external disturbances, respectively. And when the external perturbation and uncertainty information exists bounded, the two are combined into a composite disturbance, then it is shown in Eq. (12).

$$\dot{\hat{e}} = L(j)\times\left(e-\hat{e}\right) = L(j)\times\left[P_0(j)a + C_0(j,s)s + G_0 - \tau\right]\times\left(e-\hat{e}\right) - L(j)\hat{e} \tag{12}$$

In Eq. (12), $\dot{\hat{e}}$ represents the combination of external interference and uncertain parameters i.e. composite interference and $e = \tau_e - \Delta P(j)a - \Delta C(j,s)s - \Delta G(j) - F(s)$, $\hat{e}$ are the estimates of NDO for the composite interference and $L(j)$ is the gain matrix. This is then combined with the auxiliary parameter variables and function vectors to arrive at the equation design of the NDO as shown in Eq. (13).

$$\begin{cases} \dot{v} = L(j)\left[C_0(j,s)s + G_0(j) - \tau - d(s)\right] - L(j)v \\ \hat{e} = v + d(s) \end{cases} \tag{13}$$

In Eq. (13), v is an auxiliary parameter variable and $v = \hat{e} - d(s)$, $d(s)$ denote the function vectors to be designed. And the design equation of NFTSM is shown in Eq. (14).

$$h_i = g_i + \alpha_i |g_i|^{\lambda_{1i}} \times \operatorname{sgn}(g_i) + \beta_i \left|\dot{g}_i\right|^{\lambda_{2i}} \times \operatorname{sgn}\left(\dot{g}_i\right) \tag{14}$$

In Eq. (14), g_i is the joint angular velocity error, in addition $\alpha_i |g_i|^{\lambda_{1i}} \times \operatorname{sgn}(g_i)$ and $\beta_i \left|\dot{g}_i\right|^{\lambda_{2i}} \times \operatorname{sgn}\left(\dot{g}_i\right)$ are the convergence velocity states of the system and $\alpha_i > 0, \beta_i > 0$, $\begin{cases} \lambda_{1i} < \lambda_{2i} \\ 1 < \lambda_{2i} < 2 \end{cases}$. When λ_{1i} and λ_{2i} take the appropriate values, the state of the control system is non-singular. Then the Gaussian hypergeometric function and the convergence time of the error are utilized to simplify the equation design of the NFTSM, and finally the system is controlled equivalently by combining the double power convergence law and the saturation function, which in turn reduces the error estimation of the interference observer. This is shown in Eq. (15).

$$f = R^{+}\begin{Bmatrix} P_0 a_e + C_0 s + G_0 + P_0\beta^{-1}\lambda_2^{-1} \times diag\left(\left|\dot{g}_i\right|^{1-\lambda_{2i}}\right) \times \left[I + \alpha\lambda_1 \times diag\left(\left|\dot{g}_i\right|^{\lambda_{1i}-1}\right)\right] \times \dot{g} \\ + sat(h) \times \left[P_0 K \times diag\left(|h_i|^{\gamma_1}\right) + P_0 X diag\left(|h_i|^{\gamma_2}\right)\right] - \hat{e} - \omega \end{Bmatrix} \tag{15}$$

In Eq. (15), ω represents the robust term for error reduction and $\omega = -\varsigma_e \operatorname{sgn}(h)$, $K \times diag\left(|h_i|^{\gamma_1}\right)$ and $X diag\left(|h_i|^{\gamma_2}\right)$ are the stability of the system control and $K = diag(k_1, k_2, k_3), X = diag(x_1, x_2, x_3)$. Additionally, ς_e is a smaller positive number and is greater than or equal to the upper bound of the error estimate of the disturbance observer, i.e., $\|g_e\| \le \varsigma_e$.

IV. TDRA Control Combining RBF and Controller

TDRA in TT control is simulation experiments using RBF-ANN and its controller on a commercial mathematical software (Matrix Laboratory, MATLAB) platform. The study uses triple-joint RA to simulate and test the position, velocity and tendon tension curves of each joint, and then combines the approximation curves of the auxiliary system and the saturation function to compare the tracking error of the triple-joint motion. Finally, the tracking trajectories of the three joints and the estimation of the interference observations are simulatively tested using an interference observer to demonstrate the tracking accuracy and error convergence of the TDRA.

A. Trajectory Tracking Test for RBF-ANN Controller

The study uses a triple-joint RA for tendon drive and RBF-ANN for TT, whose three joints have linkage mass m specifically 0.02kg, 0.11kg and 0.13kg, and the lengths L are 0.01m, 0.04m0.05m, respectively. And for the controller the parameters include the approximation value of DM 0.3, the minimum constant of the auxiliary system 0.02, and the initial matrix parameter 0.2 and approximation value matrix parameter 1.5. The gain matrix parameter is 30. The tracking test of the joint position and velocity of the three-joint RA is carried out in the MATLAB platform, in which the results of the position tracking are shown in Fig. 5.

From Fig. 5(a), it can be inferred that joint 1's position tracking occurs with a tracking error of 0 to 0.1 degrees during the first 0.5 seconds, and joint 2's position tracking in Fig. 5(b) occurs with an error of -0.1 to 0 degrees within 0.2 seconds of the test starting. And the position tracking of joint 3 is seen in Fig. 5(c) to have a deviation of -0.1~0 degrees, occurring within 0.3 seconds of the simulation test. All three joints experience significant vibration during the initial tracking, which in turn leads to the error. However, the position tracking of the joints gradually converges to the desired tracking trajectory after 1s under the effect of the ANN controller. As for the velocity tracking results of the joints, they are shown in Fig. 6.

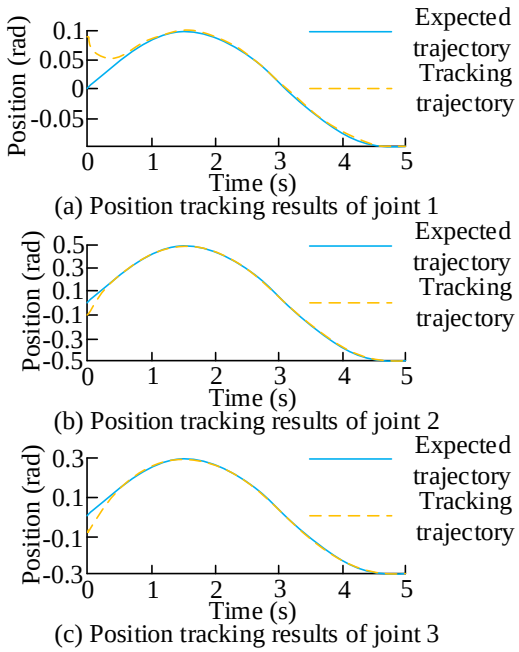

(a) Position tracking results of joint 1

(b) Position tracking results of joint 2

(c) Position tracking results of joint 3

Fig. 5. Three joint position tracking results of the robotic arm.

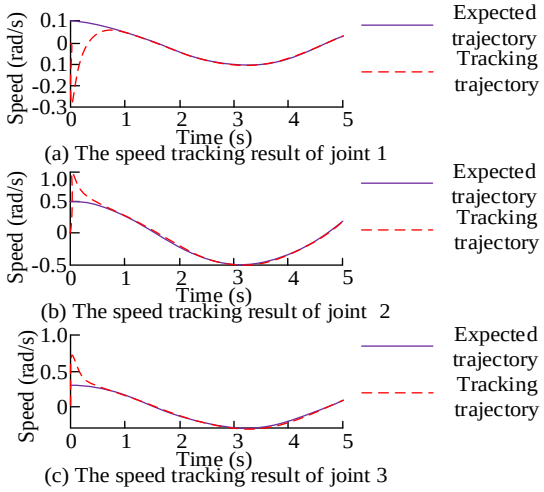

(a) The speed tracking result of joint 1

(b) The speed tracking result of joint 2

(c) The speed tracking result of joint 3

Fig. 6. Three joint velocity tracking results of the robotic arm.

From Fig. 6(a), the velocity tracking of joint 1 has an error of -0.3~0.1°/s within 0.8s and the trajectory converges to the desired trajectory after 1s. Joint 2 in Fig. 6(b) has a velocity deviation of 0~1°/s within 0.5s, and joint 3 in Fig. 6(c) has a velocity trajectory error of 0~0.8°/s within 0.5s, which results in 0~0.8°/s. All the three joints achieve a stable tracking of the trajectory after 1s, which in turn indicates that the position and velocity tracking of the joints, and the actual trajectories are able to track the desired trajectories relatively quickly under the RBF-ANN controller. Afterwards, the trajectory observation of the control moments of the three joints, as well as the error approximation test of the RBF-ANN control on the DM of the RA, are shown in Fig. 7.

The control moment curves of the three joints are seen to be smoother in Fig. 7(a), which in turn indicates that the trajectory jitter of the TDRA is not obvious. The approximation of the RA error by the RBF-NN is derived in Fig. 7(b), which converges to the true value at 14s. Where the maximum error value is 58 at the initial time, but this is due to the selection of the initial values of each parameter of the neural network, and the curve is gradually approximated with the increase of time afterwards. Therefore, it is proved that the RBF-NN based TDRA in the auxiliary system and function method can improve the tracking effect of tendon tension and the mechanical control ability, so as to improve the accurate tracking control performance of TDRA.

B. Robot Arm Trajectory Tracking Test Combined with Interference Observer

The optimized adaptive control module based on back-stepping is simulated and experimented with uncertain parameters and missing information for TDRA. And the function is combined to compare the joint tracking under different parameters, and then the disturbance observer is set to test the TT of RA. Among them, Fig. 8 displays the results of testing joint 1's position tracking under various auxiliary and stability coefficients.

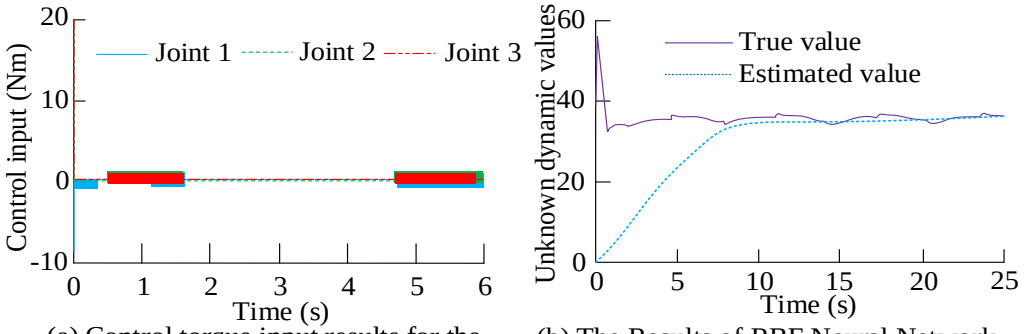

(a) Control torque input results for the three levels

(b) The Results of RBF Neural Network Approximation

Fig. 7. Results of joint control torque and controller approximation values.

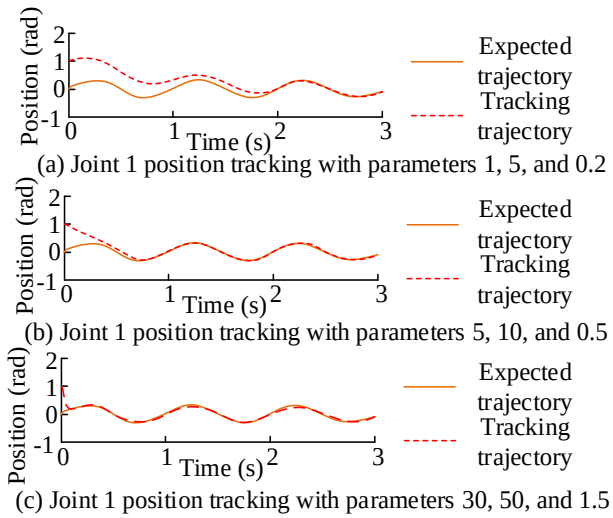

(a) Joint 1 position tracking with parameters 1, 5, and 0.2

(b) Joint 1 position tracking with parameters 5, 10, and 0.5

(c) Joint 1 position tracking with parameters 30, 50, and 1.5

Fig. 8. Joint 1 position tracking with different parameters.

In Fig. 8(a), joint 1 achieves TT stabilization after 2s and has a maximum error of 1°. It is derived in Fig. 8(b) that the coincidence with the desired trajectory is achieved after 1.8s and remains stable. Whereas, in Fig. 8(c) the curvilinear case of TT occurs when it is close to 0 i.e. 0.2s, which in turn indicates that the accuracy of TT of the joints of the RA increases with the increase in the parameters. After that, the velocity tracking test was performed for joint 2 with different parameters and the results are shown in Fig. 9.

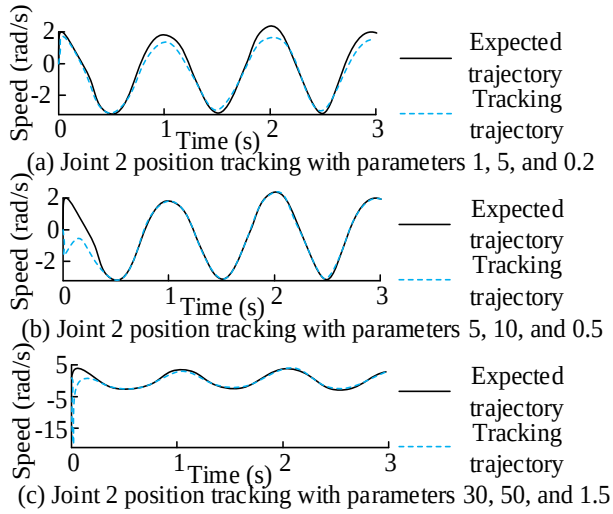

(a) Joint 2 position tracking with parameters 1, 5, and 0.2

(b) Joint 2 position tracking with parameters 5, 10, and 0.5

(c) Joint 2 position tracking with parameters 30, 50, and 1.5

Fig. 9. Joint 2 velocity tracking with different parameters.

In Fig. 9(a), the velocity tracking of joint 2 is more unstable and the error exists intermittently, in Fig. 9(b). Approximate convergence of the velocity trajectory of joint 2 occurs after 1.5s and remains TT stable. In Fig. 9(c), the velocity tracking curve of joint 2 coincides with the desired trajectory after 1.2s and the maximum error appears to be 25°/s, thus demonstrating that the increase in parameters leads to an increase in the accuracy of joint velocity tracking for RA. Finally, the position and velocity tracking of the three joints of the RA are simulated and tested under the design of the interference observer, in which the results of joint 3 are shown in Fig. 10.

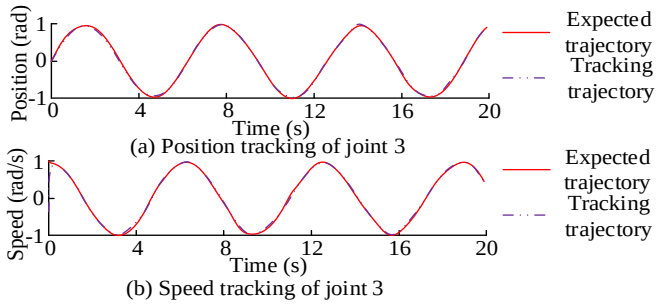

(a) Position tracking of joint 3

(b) Speed tracking of joint 3

Fig. 10. Results of Joint 3 Position and Speed Tracking

In Fig. 10(a), the position tracking of joint 3 has negligible error from the desired curve, and the TT is more stable and accurate at 0.2s. In the velocity tracking trajectory in Fig. 10(b), the trajectory coincides with the desired trajectory after 0.2s, thus indicating that the interference observer improves the accuracy and velocity of the RA joint TT. After that, regarding the interference observation results and control moments of the joints, the results of joint 2 are shown in Fig. 11.

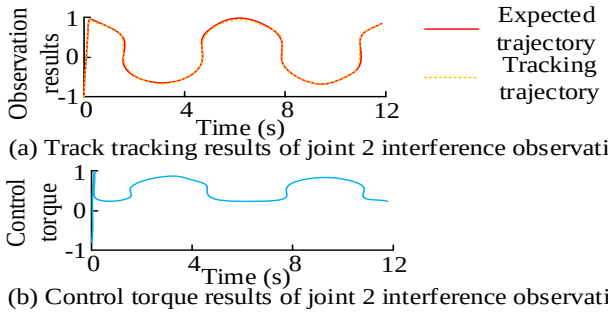

(a) Track tracking results of joint 2 interference observation

(b) Control torque results of joint 2 interference observation

Fig. 11. Interference observation results of joint 2.

In Fig. 11(a), the interference observation of joint 2 basically coincides with the desired trajectory. And the control moments of joint 2 in Fig. 11(b) change at 1.5s, 4.5s and 8s with small changes. Therefore, the interference observer has an accurate estimation of the tracking trajectory of TDRA. Finally, the curve comparison of the tendon tension change was performed, and the specific results are shown in Fig. 12.

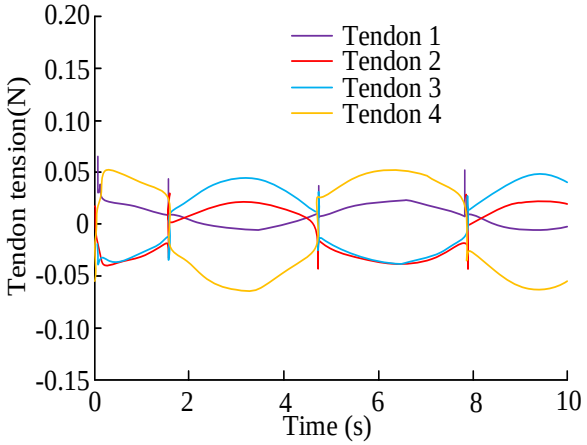

Fig. 12. Curve of tendon tension variation.

In Fig. 12, the convergence time of tendon 1 is faster, and the curve is smoother and more stable, while the tension changes of the rest of the tendons range from -0.1N to 0.1N. The changes in the tension of the remaining tendons are all affected by the compound interference, which makes the curve change more obvious ups and downs. Based on the estimated design of the disturbance observer, it is then shown that the TT controlled by the TDRA terminal sliding mode has a better performance, and thus the accuracy and convergence speed of the TT are improved under the optimization of the controller.

V. Discussion

As one of the important research directions of intelligent industrial robots, the joint angle tracking and adaptive controller design of the robotic arm control system provide key dynamic analysis for the flexible operation of the robotic arm. The study utilizes the tendon driving theory and its tendon tension constraints, and calculates the dynamic model through the Euler Lagrange equation. It also combines the dynamic relationship of the tendon driven robotic arm to clarify the specific parameters of the tendon actuator, thereby simplifying the joint activity of the robotic arm. Afterwards, using the adaptive control of RBF neural network, the tendon driven robotic arm is modeled and tracked. In addition, the adaptive law value of RBF neural network weights can reduce trajectory tracking errors and improve the accuracy of error control and positioning tracking. In order to achieve the adaptive control system and trajectory tracking of the robotic arm, the research also quotes the backstepping method to optimize the robotic arm control system. By calculating the Lyapunov function and adaptive fuzzy control law, the stability of the control system is increased. Finally, adding a nonlinear disturbance observer and NFTSM to compensate for and control trajectory errors can enable the control system to converge to the desired trajectory in a finite time, with high steady-state accuracy. However, compared with existing research on robotic arm control systems, the optimization improvement of tendon driven and adaptive RBF neural networks not only simplifies the dynamic model, but also improves the accuracy of trajectory tracking. The calculation of adaptive fuzzy control law not only considers trajectory tracking problems, but also adds technical means of adaptive movement operation to achieve intelligent development and application of robotic arms, compared to methods such as fuzzy logic control algorithm, self-anti-interference algorithm, and sensor control. In summary, the tendon drive theory and RBF adaptive neural network used in the study can efficiently and accurately improve the trajectory tracking of robotic arms. However, there is a lack of experimental platform detection and analysis for hardware failures of robotic arms in the study, and the optimization of control performance by fuzzy control rules has not been included in the analysis. Therefore, future research will extensively explore the fault detection and system parameter processing of robotic arm control performance, and play the industrial and service functions of robotic arms in medical, aviation, and military fields, thereby promoting intelligent construction and digital development.

Fundings

The research is supported by Provincial and ministerial level and above vertical scientific research projects (ZX20220460): Research and application development of key technologies for data-driven intelligent case handling.

VI. Conclusion

For the requirements of flexible operation of TDRA, the study combines tendon driven DM to construct a simplified TDRA model, and then uses RBF-NN for adaptive control of RA in order to improve RA control accuracy and stability. After that, the RA model information is refined using back-stepping method according to the parameter disturbances and model information. Finally, the interference observer is utilized to linearly estimate the mechanical energy of the interference factors, which in turn improves the accuracy and speed of joint tracking. Simulation experiments with a commercial mathematical software platform yielded that the position tracking of the three joints in the TDRA streamlined model incurred tracking position errors within 0.5s, 0.2 and 0.3s, respectively, and velocity deviations within 0.8s, 1s and 0.5s, respectively. After optimizing the controller, joint 1 experienced trajectory overlap in tracking position after 2s, 1.8s and 0.2s while joint 2 experienced trajectory overlap in tracking velocity after 1.5s and 1.2s when the parameters kept increasing. Thus, it is indicated that the accuracy of RA joint tracking gradually increases with the increase of parameters. Also under the linear estimation of the disturbance observer, the tracking trajectory of joint 3 in TDRA coincided with the desired trajectory after 0.2s. The control moments of joint 2 changed at 1.5s, 4.5s and 8s with smaller changes. And the tension curve of tendon 1 was smoother, thus proving the higher accuracy of the TDRA trajectory based on RBF-ANN. However, the study lacks data support for RA practical application experiments, and further in-depth and improvement of subsequent studies are needed.

References

[1] Yang M, Zeng G, Ren Y, Lin L, Ke W, and Liu Y. Accessibility and Trajectory Planning of Cutter Changing Robot Arm for Large-Diameter Slurry Shield. Mechanika, 2023, 29(3): 214-224. DOI:10.5755/j02.mech.30386.

[2] Wang M, Chen B, Lin C. Prescribed Finite-Time Adaptive Neural Trajectory Tracking Control of Quadrotor via Output Feedback. Neurocomputing, 2021, 458(11): 364-375. DOI:10.1016/j.neucom.2021.06.018.

[3] Duan K, Fong S, Chen C L P. Reinforcement learning based model-free optimized trajectory tracking strategy design for an AUV. Neurocomputing, 2022, 469(16): 289-297. DOI:10.1016/j.neucom.2021.10.056.

[4] Lopez-Sanchez I, Rossomando F, Ricardo Pérez-Alcocer, et al. Adaptive Trajectory Tracking Control for Quadrotors with Disturbances by Using Generalized Regression Neural Networks. Neurocomputing, 2021, 460(11): 243-255. DOI:10.1016/j.neucom.2021.06.079.

[5] Zhang W, Wang Q, Xu Z, Xu H, Ma X. An Experimental Study of the Influence of Hand-Arm Posture and Grip Force on the Mechanical Impedance of Hand-Arm System. Shock and Vibration, 2021, 2021(4): 1-11. DOI:10.1155/2021/9967278.

[6] Wang M, Li W, Luo J, and Walter U. Coordinated hierarchical control of space robotic safe manipulation with load sharing. Acta astronautica, 2023, 202(1): 360-372. DOI:10.1016/j.actaastro.2022.10.030.

[7] Korayem M H, Ghobadi N, Dehkordi S F. Designing an optimal control strategy for a mobile manipulator and its application by considering the effect of uncertainties and wheel slipping. Optimal Control Applications and Methods, 2021, 42(5): 1487-1511. DOI:10.1002/oca.2745.

[8] Zhao X. Multifeature video modularized arm movement algorithm

evaluation and simulation. Neural computing & applications, 2023, 35(12): 8637-8646. DOI:10.1007/s00521-022-08060-0.

[9] Yang C, Xie H, Xu H, Chen Y, Xu K, and Yang W. Rat-Robot Autonomous Navigation System Based on Wearable Sensors. IEEE Sensors Journal, 2023, 23(10): 11007-11015. DOI:10.1109/JSEN.2023.3263364.

[10] He Q, Zhang Q. A flexible temperature sensing finger using optical fiber grating for soft robot application. Optoelectronics Letters, 2021, 17(7): 400-406. DOI:10.1007/s11801-021-0144-0.

[11] Peng L, Zhao H, Liu R, Ding S, Wen J. Trajectory tracking control of underactuated tendon-driven truss-like manipulator based on type-1 and interval type-2 fuzzy logic approach. International Journal of Intelligent Systems, 2022, 37(6): 3736-3771. DOI:10.1002/int.22745.

[12] Matsuda Y, Sato Y, Sugi T, Goto S, Egashira N. CONTROL SYSTEM FOR A MOBILE ROBOT WITH OBJECT GRASPING ARM BY COMBINING MANUAL OPERATION WITH VISUAL SERVOING. International journal of innovative computing, information and control, 2021, 17(6): 2081-2092. DOI:10.24507/ijicic.17.06.2081.

[13] Jiang Q, Li J, Masood D. Fiber-optic-based force and shape sensing in surgical robots: a review. Sensor Review, 2023, 43(2): 52-71. DOI:10.1108/SR-04-2022-0180.

[14] Liu Y, Li X, Zhu A, Zheng Z, Zhu H. Design and evaluation of a surface electromyography-controlled lightweight upper arm exoskeleton rehabilitation robot. International Journal of Advanced Robotic Systems, 2021, 18(3): 219-232. DOI:10.1177/17298814211003461.

[15] Linxi G, Yunfei C. Human Following for Outdoor Mobile Robots Based on Point-Cloud's Appearance Model. Chinese Journal of Electronics, 2021, 30(6): 1087-1095. DOI:10.1049/cje.2021.07.017.

[16] Naya-Varela M, Duro R J, Faina A. Engineering morphological development in a robotic bipedal walking problem: An empirical study. Neurocomputing, 2023, 527(3): 83-99. DOI:10.1016/j.neucom.

[17] Fei Z M S. Torque estimation for robotic joint with harmonic drive transmission based on system dynamic characteristics. System Engineering and Electronics, 2022, 33(6): 1320-1331. DOI:10.23919/JSEE.2022.000151.

[18] C J G A B, C E K A B, D W H, H Q A C E. Adaptive model-based dynamic event-triggered output feedback control of a robotic manipulator with disturbance. ISA Transactions, 2021, 122(6): 63-78. DOI:10.1016/j.isatra.2021.04.023.

[19] Tan S, Sun L, Song Y. Prescribed performance control of Euler–Lagrange systems tracking targets with unknown trajectory. Neurocomputing, 2022, 480(6): 212-219. DOI:10.1016/j.neucom.2022.01.058.

[20] Deylami A, Izadbakhsh A. Observer-based adaptive control of cooperative multiple manipulators using the Mastroianni operators as uncertainty approximator. International Journal of Robust and Nonlinear Control, 2022, 32(6): 3625-3646. DOI:10.1002/rnc.5980.